Non-contact infrared-mediated heat transfer during continuous freeze-drying of unit doses

Pieter-Jan Van Bockstal[a], Laurens De Meyer[a], Jos Corver[a], Chris Vervaet[b], Thomas De Beer[a,*]

[a] Laboratory of Pharmaceutical Process Analytical Technology, Department of Pharmaceutical Analysis, Faculty of Pharmaceutical Sciences, Ghent University, Ottergemsesteenweg 460, 9000 Ghent, Belgium

[b] Laboratory of Pharmaceutical Technology, Department of Pharmaceutics, Faculty of Pharmaceutical Sciences, Ghent University, Ottergemsesteenweg 460, 9000 Ghent, Belgium

*Corresponding author: Thomas De Beer

Ghent University

Laboratory of Pharmaceutical Process Analytical Technology,

Ottergemsesteenweg 460

9000 Ghent (Belgium)

Tel. +32 9 264 80 97

Fax +32 9 222 82 36

E-mail: Thomas.DeBeer@UGent.be

Abstract

Recently, an innovative continuous freeze-drying concept for unit doses was proposed, based on spinning the vials during freezing. An efficient heat transfer during drying is essential to continuously process these spin frozen vials. Therefore, the applicability of non-contact infrared (IR) radiation was examined. The impact of several process and formulation variables upon the mass of sublimed ice after 15 minutes of primary drying (i.e., sublimation rate) and the total drying time was examined. Two experimental designs were performed in which electrical power to the IR heaters, distance between the IR heaters and the spin frozen vial, chamber pressure, product layer thickness and five model formulations were included as factors. A near-infrared (NIR) spectroscopy method was developed to determine the endpoint of primary and secondary drying. The sublimation rate was mainly influenced by the electrical power to the IR heaters and the distance between the IR heaters and the vial. The layer thickness had the largest effect on total drying time. The chamber pressure and the five model formulations had no significant impact on sublimation rate and total drying time, respectively. This study shows that IR radiation is suitable to provide the energy during the continuous processing of spin frozen vials.

Keywords

Freeze-drying/Lyophilization, Near-infrared spectroscopy, Principal Component Analysis, Factorial Design, Process Analytical Technology

Abbreviations

DoE: Design of Experiments, IR: infrared, MLR: Multiple Linear Regression, NIR: near-infrared, PC: principal component, PCA: Principal Component Analysis, rpm: rotations per minute, T_e: eutectic temperature, T_g: glass transition temperature, T_g': glass transition temperature of the maximum freeze-concentrated solution

Introduction

The market of biopharmaceutical drug products is strongly emerging within the pharmaceutical industry[1]. However, these macromolecules are often insufficiently stable when formulated as an aqueous solution[2]. Freeze-drying (lyophilisation) is a process frequently used to increase the stability of biopharmaceuticals during distribution and storage[3]. Traditional pharmaceutical freeze-drying is a batch-wise process: all vials of the same batch are processed through a sequence of consecutive process steps (i.e., freezing, primary and secondary drying) until the final dried product is achieved. The temperature-controlled shelves in the drying chamber are loaded with glass vials (i.e., unit doses) containing the aqueous drug formulation. The freezing step is initiated by gradually decreasing the temperature of these shelves, resulting in the conversion of most of the water into ice. Ice formation is associated with a gradual increase in solute concentration between these ice crystals, leading to crystallisation of these solutes or to the formation of an amorphous glass. During primary drying, the pressure in the drying chamber is lowered, conventionally between 5 and 30 Pa, and the shelf

temperature is increased which allows ice sublimation to take place. Finally, during the secondary drying step, remaining unfrozen water is eliminated by desorption until the desired residual moisture content is achieved. At the end of the lyophilisation process, the aqueous solution of the (heat-)labile biopharmaceutical is hence transformed into a solid, dry cake with an increased shelf-life.

Conventional batch freeze-drying is inherently associated with several disadvantages. The traditional lyophilisation process is inefficient and time- and energy-consuming[3]. Cycle times can vary from 1 to even 7 days, depending on several factors like formulation characteristics (e.g., glass transition temperature of the maximum freeze-concentrated solution (T_g') and dried product mass transfer resistance) and vial type. The processing of industrial batches, often containing thousands of vials, leads to operational risks, mainly during loading and unloading of the drying chamber due to complicated handling of the vials. The handling equipment in the steps before (filling) and after (capping, packaging) freeze-drying is continuously operated by nature. Both before (filling) and after (capping, packaging) freeze-drying, this handling equipment is naturally operated in a continuous manner. Therefore, buffer systems are required to bridge the time until the start of the upcoming cycle, which highly increases the risk of product contamination. Additionally, the handling equipment and buffer systems take up an enormous space which must meet the class 100 clean room standards, mandatory in the sterile production of (injectable) biopharmaceuticals[4]. These strict requirements in terms of sterility and cleanliness strongly increase production costs.

The huge size of industrial batches is impractical for cycle development. The initial development of freeze-drying cycles is performed in lab-scale equipment. Subsequent steps in the development process demand scale-up from lab-scale to pilot-scale and, finally, to industrial-scale freeze-driers. Differences in heat and mass transfer between each equipment scale require re-optimisation and re-validation of these cycles[5,6]. Also, in general, the freeze-drying equipment is designed and optimised to process the maximum applicable amount of vials. Often, the required batch size is smaller than the maximum load, leading to inefficient use of the equipment. Additionally, re-validation of the freeze-drying cycle is mandatory in case the batch size is modified.

During the freezing stage in batch freeze-drying, ice nucleation generally does not occur at the equilibrium freezing point of the solution. Retaining the liquid state below the equilibrium freezing temperature is a phenomenon termed supercooling[7]. Ice nucleation during traditional batch freeze-drying is a stochastic event, resulting in different degrees of supercooling for each vial in the batch. A higher degree of supercooling leads to a higher rate of ice nucleation and a faster effective freezing rate[7]. This way, a high number of small ice crystals is obtained. In turn, a lower degree of supercooling results in less large ice crystals. The stochastic nature of ice nucleation during batch freeze-drying leads to different sizes of ice crystals in each vial of the batch. The ice crystal size in the frozen matrix corresponds to the final pore size in the dried layer during the sublimation process. As a reduced pore size is associated with a higher dried product mass transfer resistance and vice versa, the sublimation rate during primary drying is highly influenced by the pore size in the dried layer[6]. Eventually, the uncontrolled freezing step causes vial-to-vial variability of the sublimation rate within a batch and between batches[8].

Primary drying requires appropriate and sufficient energy supply to the vial, necessary for ice sublimation[3]. In the traditional batch freeze-drying concept this energy is provided via thermal conduction from the shelf to the vial by increasing the shelf temperature. Vials placed at the edge of the shelves receive additional energy radiated from the warmer surroundings (e.g., the door and walls of the drying chamber)[9]. This results in a higher temperature of these vials, associated with faster drying rates and a higher risk for collapse[5]. Both the uncontrolled freezing and the uneven heat transfer lead to different process conditions for each individual vial in the batch[7,10]. This uncontrolled vial-to-vial variation does not meet the most recent guidelines issued by the regulatory authorities[11].

Continuous manufacturing strongly increases process efficiency and improves product quality (consistency)[12]. Similar to solid dosage forms, continuous manufacturing is also of major importance for biopharmaceutical products[1,13]. Recently, an innovative continuous freeze-drying concept was proposed which tackles the higher outlined disadvantages associated with the traditional lyophilisation process[14,15]. A major difference compared to conventional batch freeze-drying concerns the freezing step: each vial is rotated along the longitudinal axis while a flow of a cold, inert and sterile gas is used to induce ice nucleation (spin freezing). Consequently, the frozen product is spread over the entire inner vial wall, resulting in a significant reduction of the product layer thickness. For the final stage of the continuous freezing step, the vial is transferred to a chamber with a controlled temperature. Here, the desired morphological structure of the ingredients can be obtained by annealing under specific process conditions[7].

An efficient heat transfer during primary drying is crucial for the continuous processing of spin frozen vials. Due to the increase of the surface available for sublimation and the corresponding reduction of the layer thickness, the primary and secondary drying efficiency can be highly improved compared to batch freeze-drying[15]. To achieve a homogeneous and efficient drying behaviour, the thin product layer requires an adequate and uniform heat transfer towards the entire vial wall. The energy necessary for sublimation can be provided through conduction by individual pockets for each vial, allowing individual temperature-regulation[14]. Alternatively, non-contact energy provision via infrared (IR) radiation could offer major benefits as opposed to the inefficient heat transfer during traditional batch freeze-drying. IR radiation is a type of electromagnetic radiation allowing energy transport between two bodies with a different absolute temperature which are not in direct contact[16]. This mechanism could be applied to provide the heat transfer to the spin frozen vials during the primary and secondary drying step of the continuous concept (Figure 1). The application of IR radiation offers a major advantage as energy is provided to the vials without direct contact with the heat source. This way it is not necessary to envelop processed vials by heatable pockets and this eases the monitoring of the drying progress at the level of each individual vial. Additionally, several vial types can be processed without the need to adapt the heatable pockets to obtain a homogeneous energy transfer[15].

The high potential and added value of IR mediated heat transfer to the continuous freeze-drying concept has to be thoroughly evaluated. The aim of this study was to test whether IR radiation is applicable for the primary and secondary drying of spin frozen vials. The influence of various process and formulation parameters upon the mass of sublimed ice after 15 minutes of primary drying (i.e.,

sublimation rate) and the total drying time was evaluated. This study is the first step in the evaluation of the feasibility of IR mediated heat transfer in the continuous processing of spin frozen vials.

Materials and methods

Experimental set-up

A 10 mL type I glass vial (Schott, Müllheim, Germany) containing the required volume of a specific formulation was vertically rotated along its longitudinal axis in a vial holder at approximately 2900 rpm. As a result, the product was spread across the whole vial wall, after which the rotating vial was immersed into liquid nitrogen for 40 ± 5 s to completely solidify the product. After spin freezing, the vial was transferred from the vial holder to the drying chamber within 15 ± 5 s, ensuring that the T_g' or eutectic temperature (T_e) of the formulation was never exceeded. The applied vertical rotation speed of 2900 rpm resulted in a homogeneous product layer with a maximum deviation of the layer thickness from top to bottom of less than 10% as calculated by:

$$\Delta l = \frac{hg}{2\pi\omega^2\sqrt{r_{v,i}^2 - \frac{V}{\pi h}}}$$

with Δl the deviation to the average thickness of the spin frozen layer (m), h the height of the spin frozen layer (m) (Figure 1), g the gravitational acceleration (9.80665 m s^{-2}), ω the angular velocity (radians s^{1}), $r_{v,i}$ the inner radius of the glass vial (m) and V the filling volume (m^3).

After spin freezing, drying was performed in the drying chamber of an Amsco FINN-AQUA GT4 freeze-dryer (GEA, Köln, Germany) with the shelves pre-cooled at -10°C. The experimental set-up consisted of two IR heaters (Weiss Technik, Zellik, Belgium) facing each other (Figure 2). The spin frozen vial was placed exactly in between these IR heaters at a defined distance. The vial was continuously rotating at a constant velocity of 5 rpm which was necessary to obtain a homogeneous energy transfer from the IR heaters to the vial. Immediately after transferring the vial to the drying chamber, the pressure was decreased until the desired vacuum was reached. Within 5 minutes the pressure in the drying chamber was below the triple point of water, avoiding exceeding the T_g' or T_e of the formulation. After exactly 17 minutes, the time necessary to achieve the desired pressure level, the IR heaters were activated. In a first series of experiments (see further), the system was aerated exactly 15 minutes after activation of the IR heaters. Immediately thereafter, the amount of sublimed ice was determined gravimetrically. In a second series of experiments, the process was stopped after secondary drying was finished.

Experimental design methodology

A D-optimal interaction screening design consisting of 36 experiments, expanded with 2 double centre points, was developed using MODDE Pro (Version 11.0.0, Umetrics, Umeå, Sweden) to evaluate the first response, i.e. the mass of sublimed ice after 15 minutes of primary drying. The length of this time span was decided during preliminary experiments to make sure sublimation was not finished within

this period. The factors examined in this first design, from now on referred to as Design of Experiments (DoE) 1, are listed in Table 1, including their examined lowest and highest level, while an overview of all individual experiments is given in Table 2. The electrical power supplied to the IR heaters is expressed in units of watt, calculated by the product of the electric current *I* and the voltage *U* provided by the voltage source. This value is a measure for the temperature of the IR heaters. The volume of each formulation to obtain the desired layer thickness was calculated based on the dimensions of the 10 mL type I glass vials. A layer thickness of 0.5, 1.0 and 1.5 mm corresponds respectively to a volume of 1.35 , 2.65 and 3.90 mL. The distance between the IR heaters and the vial is defined from the edge of the vial.

The first four variables in Table 1 are quantitative factors which can be set according to a continuous scale. The last factor, the five different model formulations used during the experiments, is a qualitative factor. An overview of the different formulations is provided in Table 3. These formulations were selected from previous studies because they have a different dried product mass transfer resistance profile in function of the dried layer thickness[17,18]. Formulations 1 and 5 were used for the centre points of DoE 1. Trehalose was obtained from Cargill (Krefeld, Germany). Polysorbate 20, sodium chloride, lactose and mannitol were purchased from Fagron (Waregem, Belgium). L-Histidine and glycine were acquired from Sigma-Aldrich (Saint Louis, MO, USA). Sucrose was purchased from VWR (Leuven, Belgium).

Similar to DoE 1, a second D-optimal interaction screening design was developed, resulting in 28 experiments with additional 2 double centre points, to evaluate the primary, secondary and total drying time and the transition width between primary and secondary drying. Comparison of the primary and total drying time will emphasize the differences between the tested model formulations, which allows a more appropriate evaluation of the impact of the dried product mass transfer resistance on the primary drying behaviour. While in DoE 1, because of the constant time interval, only differences in product resistance at the top of the cake would lead to a significant effect on the sublimation rate. An overview of the examined factors for this second experimental design, from now on referred to as DoE 2, is provided in Table 4. All experiments of DoE 2 are listed in Table 5. In this design the same factors were examined as in the former one, except for the chamber pressure, which was kept constant at 20 Pa during each experiment. The reason for this will be explained in the results section. Both the endpoint of primary and secondary drying were determined via in-line near-infrared (NIR) spectroscopy[19,20]. Hence, as opposed to DoE 1, the drying process was not interrupted during primary drying, but continued until secondary drying was finished. Similar to DoE 1, formulations 1 and 5 were used for the centre points.

MODDE Pro was used for the analysis of both experimental designs. Regression models for each response were calculated by Multiple Linear Regression (MLR)[21]. All factors were scaled and centred, which makes the regression coefficients for the different factors comparable. Each quantitative factor was set to *+1* and *-1* for their highest and lowest value, respectively. Qualitative factors require an alternative approach via a mathematical re-expression (regression coding). A *k*-level qualitative parameter will be expanded into *k-1* artificial categorical variables, as illustrated for the qualitative

factor Formulation (*For*) in Table 6. Each expanded term results in one regression coefficient, which in our case led to four coefficients for level 2 to level 5 (regular mode). Additionally, the level 1 coefficient can be calculated as the negative sum of the coefficients of the other expanded terms (extended mode). The response of the first design was described by the following extended equation:

$$y = b_0 + b_1P + b_2Dis + b_3Pc + b_4Lpr + b_5For(For1) + b_6For(For2) + b_7For(For3) + b_8For(For4) + b_9For(For5) + b_{12}PDis + b_{13}PPc + b_{14}PLpr + b_{15}PFor(For1) + b_{16}PFor(For2) + b_{17}For(For3) + b_{18}For(For4) + b_{19}For(For5) + b_{23}DisPc + b_{24}DisLpr + b_{25}DisFor(For1) + b_{26}DisFor(For2) + b_{27}DisFor(For3) + b_{28}DisFor(For4) + b_{29}DisFor(For5) + b_{34}PcLpr + b_{35}PcFor(For1) + b_{36}PcFor(For2) + b_{37}PcFor(For3) + b_{38}PcFor(For4) + b_{39}PcFor(For5) + b_{45}LprFor(For1) + b_{46}LprFor(For2) + b_{47}LprFor(For3) + b_{48}LprFor(For4) + b_{49}LprFor(For5)$$

where *y* is the response variable, *P* is the electrical power supplied to the IR heaters, *Dis* is the distance between the IR heaters and the vial, *Pc* is the chamber pressure, *Lpr* is the thickness of the product layer, *For(For1)*, *For(For2), For(For3), For(For4)* and *For(For5)* are the expanded model terms related to the qualitative factor Formulation and b_0, b_1, b_2, b_3, b_4, b_5, b_6, b_7, b_8, b_9, b_{11}, b_{12}, b_{13}, b_{14}, b_{15}, b_{16}, b_{17}, b_{18}, b_{19}, b_{23}, b_{24}, b_{25}, b_{26}, b_{27}, b_{28}, b_{29}, b_{34}, b_{35}, b_{36}, b_{37}, b_{38}, b_{39}, b_{45}, b_{46}, b_{47}, b_{48} and b_{49} are regression coefficients. Each response of DoE 2 was described by a similar equation, in which the regression coefficients for the factors and factor interactions involving *Pc* (b_3, b_{13}, b_{23}, b_{34}, b_{35}, b_{36}, b_{37}, b_{38} and b_{39}) were equal to zero because this factor was considered constant during all experiments. The regression coefficient of a specific factor represents the quantitative change in response value when this factor is increased from its average to its high level, keeping all other factors at their average value. The effect of a specific factor is defined as the quantitative change in response value when this factor is increased from its low to its high level, keeping all other factors at their average value. Based on these definitions, the effect of a factor is twice the corresponding coefficient. The constant term, b_0, is related to the response value at the design centre point, with all factors at their average level. For all regression coefficients the 95% confidence interval was calculated. Factor or interactions between factors were considered significant if the 95% confidence interval of the corresponding regression coefficient did not contain zero.

NIR spectroscopy

Diffuse reflectance NIR spectra were continuously in-line collected with an Antaris™ II Fourier-Transform NIR spectrometer (Thermo Fisher Scientific, Erembodegem, Belgium), equipped with a quartz halogen lamp, a Michelson interferometer and an InGaAs detector. The fibre optic probe was implemented in the drying chamber at a distance of 0.5 ± 0.1 mm near the base of the vial without hampering or disturbing the rotation of the vial (Figure 2). As drying progresses from the centre of the vial to the inner vial wall, in-line NIR spectroscopy allowed the detection of complete ice and water removal, i.e. the endpoint of primary and secondary drying, respectively. Every 20 seconds a NIR spectrum was collected in the 4500-10000 cm^{-1} region with a resolution of 16 cm^{-1} and averaged over 4 scans. The illumination spot size obtained with the NIR probe was approximately 28 mm^2. Due to rotation of the vial during the measurements, each spectrum was collected at a different position of the

cake on a specific height. It was assumed that this monitored part is representative for the whole cake, due to the uniform layer thickness over the entire vial wall.

Multivariate data analysis

The collected NIR spectra were separately analysed for each individual experiment of DoE 2 using the multivariate data analysis software SIMCA (Version 14.0.0, Umetrics, Umeå, Sweden). The NIR spectra collected before activation of the heaters were removed from each dataset. The Savitzky-Golay filter was applied to smooth the spectra: a quadratic polynomial function was fitted to a moving sub-model, each containing fifteen data points. Additionally, Standard Normal Variate preprocessing was applied to eliminate the additive baseline offset variations and multiplicative scaling effects in the spectra which may be caused by small variations in distance between the NIR probe and the rotating glass vial and possible differences in product density[22]. Principal Component Analysis (PCA) was then used for the analysis of the preprocessed and mean-centred NIR spectra.

PCA is an unsupervised multivariate projection method which extracts and displays the variation in the data set[23,24]. The original variables, e.g. the individual wave numbers of the NIR spectra, are replaced by a new set of latent variables, named principal components (PCs). These PCs are sequentially acquired by an orthogonal, bilinear decomposition of the data matrix. Each component explains most of the remaining variability in the data. PCs are composed of a score and a loading vector. The score vector contains a score value for each spectrum, which describes its quantitative relation to the other spectra. The loading vector provides qualitative information about which spectral features present in the original observations are captured by the corresponding component.

Results and discussion

Analysis of DoE 1

The absolute mass of ice sublimed after 15 minutes of primary drying of the individual experiments ranged from approximately 0.5 g up to 1.2 g. This corresponded to a relative amount of 36.5% up to 80% and 15% up to 30% of the total ice mass for the thinnest and thickest product layers, respectively. Evaluation of the raw data (responses) indicated there were no peculiarities in the results: the variability in sublimed ice mass between the repeated experiments was much less than the overall variability of all DoE 1 experiments. Also, data transformation before regression analysis was not needed, due to the normal distribution of the response data. The regression coefficients, computed via MLR fitting, are displayed for each factor and factor interaction, including the 95% confidence interval, in the extended coefficient plot (Figure 3).

The electrical power supplied to the IR heaters was the factor with the highest influence on the amount of sublimed ice, with a regression coefficient b_1 of 0.13966 g (Figure 3). Increasing the electrical power from 14 to 36 W, keeping all other factors at their average, hence leads to an increase of 0.279 g or 45% in the amount of sublimed ice. An increase of the electrical power can be associated with a higher temperature of the IR heater. More radiant energy was provided to the spin frozen vial, which

explains the faster ice removal. The distance between the IR heaters and the glass vial had a large, negative impact on the response variable (regression coefficient b_2 = -0.12478 g) (Figure 3). Altering the distance between the IR heaters and the glass vial from 2 to 6 cm was associated with a decrease of 0.250 g or 39% in the mass of sublimed ice, with all other factors at their average level. The efficiency with which the IR heaters provided energy to the glass vial was influenced by the view factor. The view factor is a measure of the fraction of radiation emitted by the IR heaters that hits the glass vial[25]. This dimensionless number, between 0 and 1, is only determined by the geometric orientation of both surfaces (i.e., the IR heater and the glass vial). A larger distance between the IR heaters and the glass vial decreased the view factor. Therefore, a smaller part of the emitted energy reached the vial, which resulted in the lower sublimation rate.

The chamber pressure had no significant impact on the response value (regression coefficient b_3 = -0.015711 g) (Figure 3). The energy transfer via IR radiation does not require direct contact and is mainly determined by the temperature difference between the IR heater and the spin frozen vial, given by the Stefan-Boltzmann equation[25]:

$$P = A\varepsilon F\sigma(T_h^4 - T_v^4)$$

with P the power radiated by the IR heater to the spin frozen vial (W), A the surface of the IR heater (m^2), ε the emissivity of the IR heater (-), F the view factor (-), σ the Stefan-Boltzmann constant (5.67 10^{-8} W m^{-2} K^{-4}), T_h the temperature of the IR heater (K) and T_v the temperature of the vial (K). The energy flux via IR radiation is not influenced by the gas density between the vial and the heat source, which resulted in the insignificant impact of the chamber pressure on the sublimation rate. However, when the energy transfer to spin frozen vials is provided by conduction, the chamber pressure does have a significant impact on the sublimation rate[15]. As opposed to heat transfer by radiation, direct contact is required for conductive heat transfer. Due to suboptimal contact between the stainless steel shelf and the aluminium vial holder and between this vial holder and the spin frozen vial, the conduction heat flux is enhanced with the increase in the amount of gas molecules between these surfaces. Hence, the higher heat transfer is responsible for the increased sublimation rate observed at a higher pressure[15]. This phenomenon is also extensively described in batch freeze-drying: poor contact between the shelf and the bottom of the glass vials yields a higher heat transfer coefficient when the chamber pressure is increased[3,26]. Naturally, improvement of the contact between the vial and the energy source (i.e., adaptable heatable pockets) will result in a conduction heat flux which is independent of the chamber pressure[14].

The layer thickness had a statistically significant impact on the sublimation rate (regression coefficient b_4 = 0.043128 g) (Figure 3). Tripling the layer thickness from 0.5 to 1.5 mm was associated with an increase of 0.0863 g or 12% in the mass of sublimed ice, keeping all other factors at their average. Compared to other significant factors, the influence of layer thickness is relatively low, because each experiment was stopped after a fixed drying time (15 minutes) before primary drying was completely finished. Therefore, the small impact of this factor was considered irrelevant. Five different model formulations were included in the experimental design, but only Formulation 1 had a small, statistically

significant influence, as the sublimation rate was lower in comparison with the other formulations (regression coefficient b_5 = -0.062509 g) (Figure 3). This formulation contained a higher concentration of solutes compared to the four other formulations (Table 3), which could be associated with a higher dried product mass transfer resistance and a corresponding lower sublimation rate. These results do not match the product resistance profiles in function of the dried layer thickness provided from literature[17,18]. However, these resistance profiles were determined under different process conditions for both freezing and primary drying, which impacts the pore size of the dried cake and therefore the dried product mass transfer resistance[6,27]. For this reason, the literature values might not be representative for the thin layers, obtained under the applied process conditions. Finally, comparison of the total drying time for each formulation (DoE 2) should allow a more appropriate evaluation of the impact of the dried product mass transfer resistance on the drying behaviour (see further).

Only the interaction between the factors electrical power and the distance between the IR heaters and the vial was statistically significant (regression coefficient b_{12} = -0.066907 g) (Figure 3). However, the interaction plot shows that it was only a weak interaction because both lines do not cross and there is only a small difference in slope (Figure 4). With the increase of the distance between the glass vial and the IR heaters, the influence of the electrical power provided to the IR heaters (i.e., temperature of the IR heaters) on the sublimation rate was reduced. This interaction is explained by the view factor, which decreased non-linearly with a larger the distance between IR heaters and vial[25].

Analysis of DoE 2

NIR process analysis

The PC 1 versus PC 2 score scatter plot obtained after PCA of the preprocessed NIR spectra collected during one of the individual experiments of the second design (Experiment 5 of DoE 2), is shown in Figure 5. The main part of the spectral variability (92.6%) was explained by PC 1, a smaller part of the variability was explained by PC 2 (5.39%). In the loading line plots of both PCs several NIR bands were identified (Figure 6). The band near 4760 cm^{-1} in both PC 1 and 2 stems from the combination of O-H bending and C-O stretching of trehalose, the main component of Formulation 1 (Table 3)[28]. The band directed downwards near 5130 cm^{-1} in the loading plot of PC 1 originates from O-H stretching and H-O-H bending vibrations of water[29]. Similarly, the band directed upwards near 5130 cm^{-1} in the loading plot of PC 2 could also be assigned to water. The broad band directed downwards between 5500 cm^{-1} and 7000 cm^{-1} in the loading plot of PC 1 represents the change in the ice and water signal. The band directed upwards in the loadings of PC 2 near 6640 cm^{-1} originates from symmetric and asymmetric stretch of the water molecules. The loadings of both PCs clearly represent the changes in ice and water content in the sample. Analysis of the collected spectra allowed the full explanation of the chronological trends in the score plot and the link with the drying behaviour.

The NIR spectra at the start of the primary drying process were dominated by overwhelming ice bands, which indicated the presence of ice in the monitored vial (Figure 5 and 7a). With the progress of primary drying, there is a clear trend in the scores in PC 2, as they move along the vertical axis in

the positive direction of PC 2 (Figure 5). This trend is visualized in the corresponding spectra (Figure 7a). The NIR bands near 5100 cm^{-1} and 6640 cm^{-1} gradually increase in intensity and become more distinct in shape with the progression of primary drying. These findings are confirmed by the loading line plot of PC 2, where both these bands are directed upwards (Figure 6). Ice sublimation progresses from the centre of the vial towards the inner vial wall, while NIR spectra were collected from the outside of the vial wall. The NIR light only penetrates the sample for a limited distance. Ice signals overwhelm the NIR spectra until the gradual decrease in ice layer thickness allowed the visualisation of the product, specifically the presence of residual water, besides the remaining ice signals. With further drying, the water band near 5130 cm^{-1} became more clear and a characteristic product band near 4760 cm^{-1} (i.e., trehalose) started to appear, as visualized in the spectra situated after the first inflection point in the score plot (Figure 5 and 7b). Simultaneously, ice signals weakened, but they were only completely absent in the NIR spectra displayed after the second inflection point in the score plot (Figure 5 and 7c). So, only at this point all ice crystals were completely sublimed and primary drying was finished at the monitored height of the vial which is considered to be representative for the whole cake. With the reduction of the ice signals, the trehalose band near 4760 cm^{-1} increased in intensity. The small decrease in the water band near 5130 cm^{-1} is attributed to the fact that secondary drying occurs simultaneously with primary drying in ice-free regions[3]. The loadings of PC 1 confirmed this (Figure 6). The band assigned to trehalose is directed in the upwards direction while the bands assigned to water and ice are directed downwards. Therefore, the spectra, represented by scores, situated at the right side along the horizontal axis in the score plot contained less water and ice (Figure 5). In the subsequent NIR spectra, the water band at 5130 cm^{-1} gradually decreased along both PC 1 and 2 until the spectra started to cluster (Figure 5 and 7d). At this point the residual moisture stabilised, secondary drying was finished and the final dried product was obtained. This decrease in water content is confirmed by the loading plots of both PC 1 and 2 (Figure 6). The water band at 5130 cm^{-1} is directed downwards in the loading plot of PC 1 and the cluster of spectra is situated at the right side along the horizontal axis. The same water band is directed upwards in the loading plot of PC 2 and the cluster of spectra is situated at the bottom along the vertical axis.

In the score scatter plot, NIR spectra were identified in which drying had not progressed as much as in spectra collected earlier in the process. To achieve a homogeneous heat transfer, IR radiation requires the rotation of spin frozen vials during drying. As a result, each spectrum was recorded at a different, horizontal position at one specific height of the vial. This indicated that the drying progress was not completely homogeneous for the whole monitored region, although energy was equally provided. Consequently, primary drying was locally finished at different time points, which is visualised in the PC 1 versus time plot (Figure 8). This plot shows to which extent the drying behaviour was homogeneous or not. The inhomogeneous primary drying behaviour might be explained by small deviations in layer thickness or by local differences in dried product mass transfer resistance. This effect was not observed at the end of secondary drying.

For all individual experiments the score scatter plot showed the same trends and therefore they were all analysed in a similar way. The several responses studied in the second design (end of primary

drying, end of secondary drying, total drying time, transition width between primary and secondary drying) could be determined based on this PCA plot. The primary drying time was defined as the time between the collection of the first spectrum after the onset of the heaters and the spectrum following the last spectrum situated before the second inflection point in the score plot. The total drying time was defined as the time between the collection of the first spectrum after the onset of the heaters and the spectrum following the last spectrum situated outside of the cluster where secondary drying is finished. The secondary drying time was computed as the difference between the total drying time and the time necessary for primary drying. Additionally, for each run the PC 1 versus time plot was analysed to determine the time between the first monitored position of the cake primary drying was finished and the point sublimation was completely finished. This transition width was added as a response to the analysis of DoE 2 and was defined as the time between the first spectrum after the second inflection point and the spectrum following the last spectrum situated before the second inflection point in the score plot.

Factor and interaction significance analysis

Each response of DoE 2 was analysed in a similar way to the response of DoE 1. There were no peculiarities in the raw data: for each response the variability between the repeated experiments was much less than the overall variability of all DoE 2 experiments. The regression coefficients for each response are shown in the extended coefficient plots (Figure 9, 10 and 11)

The total drying time ranged for the individual experiments from approximately 20 minutes up to 175 minutes. The total drying rate was mainly influenced by the thickness of the product layer, with a regression coefficient b_4 of 33.78 min (Figure 9). Tripling the layer thickness from 0.5 to 1.5 mm was associated with an increase in total drying time of 67 min or 169%, keeping all other factors at their average level. The influence of the layer thickness was much larger because the drying process was continued until a dried end product was obtained as opposed to DoE 1, where primary drying was interrupted after 15 minutes. The impact of the electrical power (regression coefficient b_1 = -17.795 min) and the distance between IR heaters and glass vial (regression coefficient b_2 = 18.543 min) on the drying progress confirmed the results of DoE 1 (Figure 9). Increasing the electrical power from 14 to 36 W reduced the total drying time with 35 min or 39% and positioning the IR heaters at a distance of 2 cm instead of 6 cm from the glass vial decreased the total drying time with 37 min or 40%, keeping all other factors at their average. Naturally, these three process variables had the same impact on the primary and secondary drying time (Figure 10 and 11). Because the absolute time required for secondary drying is shorter in comparison to the primary and total drying time, the effect of each significant factor on the secondary drying time is less pronounced.

Formulation 4 was the only formulation which had a statistically significant impact on the primary drying rate with a regression coefficient b_8 of 5.3987 min (Figure 10), although all formulations had a different dried product mass transfer resistance profile according to literature values[17,18]. Lower primary drying rates for lactose solutions have been reported earlier and could be explained by the formation of a low permeable skin at the top of the cake which is associated with a high product

resistance[15,30]. Due to the compensation by faster secondary drying of formulation 4, none of the five model formulations had a significant impact on the total drying time (Figure 9). This confirms the theory that product resistance plays a less crucial role in the primary drying behaviour of spin frozen vials in comparison with traditional freeze-drying due to the thinner product layers[15].

Several significant factor interactions were identified for the total, primary and secondary drying time (Figure 9, 10 and 11). However, based on the analysis of the interaction plots similar to Figure 4, we could conclude that there were no strong, relevant interactions between the factors.

The transition width varied from 20 seconds to 17 minutes. Only two factors had a significant impact on this response variable. A larger distance between the IR heaters and the glass vial was associated with a longer transition width (regression coefficient b_2 = 2.6107 min) as this prolonged the total drying time, which simultaneously increased the transition width. A thicker product layer also significantly impacted the transition width (regression coefficient b_3 = 1.7261 min), also linked to a longer drying time.

The aim of DoE 2 was to determine the impact of several process and formulation variables on the drying time. The design was not specifically performed to study the transition width between primary and secondary drying. This response was only added after analysis of the NIR data of the individual experiments of DoE 2. Therefore, the included factors were not optimal to study this response, which might explain why only two factors had a significant impact on this response.

Conclusion and future perspectives

IR radiation is highly suitable to provide the energy necessary for the continuous processing (i.e., drying) of spin frozen vials. The electrical power supplied to the IR heaters and the distance between the IR heaters and the glass vial, were the most influential factors on the sublimation rate. Additionally, the layer thickness had the largest impact on the total drying time. The pressure in the drying chamber had no significant effect on the sublimation rate in contrast to energy provision via conduction during both batch and continuous freeze-drying. Although several formulations with a different dried product resistance profile were tested, no significant differences in total drying time were observed. This might indicate that dried product mass transfer resistance is less crucial in the primary drying behaviour of spin frozen vials compared to batch freeze-drying, due to the reduced product layer thickness. Further research is necessary to confirm this finding.

A NIR spectroscopy method was developed to monitor the drying behaviour of spin frozen vials. This method allowed the visualisation of the drying progress and the determination of the endpoint of both primary and secondary drying. Additionally, it was possible to determine the homogeneity of the primary drying behaviour within the vial. During traditional batch freeze-drying, only one vial of the batch, or a few vials in case of a multipoint set-up, can be monitored in-line with NIR spectroscopy[9,31]. Also, the monitored vial(s) are often not representative for the whole batch. A continuous moving belt of spin frozen vials counters these disadvantages and allows the monitoring of each individual vial in a representative way. The NIR measurements were accomplished while the vial was continuously

rotating and therefore the spectra cover a large portion of the product. Also, the penetration depth of the light of the NIR probe is only a few tenths of a millimetre and since relatively thin layers are applied in this process, the measurement results are more representative compared to current methods in batch freeze-drying.

Cake appearance is one of the Critical Quality Attributes of freeze-dried products[7]. Limitation of the IR energy transfer to spin frozen vials to ensure that both T_g' and the glass transition temperature (T_g) are not exceeded during respectively primary and secondary drying, is of major importance to maintain an appropriate cake appearance. Therefore, it is necessary to develop mechanistic models, similar to batch freeze-drying, which allow to calculate the maximum allowable energy transfer to the spin frozen vials, avoiding cake collapse during processing, but ensuring as efficient as possible drying[27,32]. Additionally, these models should be able to predict the amount of sublimed ice and the endpoint of the primary drying step. This is an essential step in the development of the continuous freeze-drying concept.

References

1. Kasper, J. C., Winter, G. & Friess, W. Recent advances and further challenges in lyophilization. *Eur. J. Pharm. Biopharm.* **85,** 162–169 (2013).

2. Constantino, H. R. & Pikal, M. J. *Lyophilization of Biopharmaceuticals*. (AAPS Press, 2004).

3. Jennings, T. *Lyophilization: Introduction and basic principles*. (Informa healthcare, 2008).

4. Tschudi, W., Benschine, K., Fok, S. & Rumsey, P. Cleanroom Energy Benchmarking In High-Tech and Biotech Industries. in *ACEEE Summer Study on Energy Efficiency in Industry, July 24-27, 2001, published in the Proceedings.*

5. Rambhatla, S. & Pikal, M. J. Heat and mass transfer scale-up issues during freeze-drying, I: atypical radiation and the edge vial effect. *AAPS PharmSciTech* **4,** 22–31 (2003).

6. Rambhatla, S., Ramot, R., Bhugra, C. & Pikal, M. J. Heat and mass transfer scale-up issues during freeze drying: II. Control and characterization of the degree of supercooling. *AAPS PharmSciTech* **5,** 54–62 (2004).

7. Kasper, J. & Friess, W. The freezing step in lyophilization: physico-chemical fundamentals, freezing methods and consequences on process performance and quality attributes of biopharmaceuticals. *Eur. J. Pharm. Biopharm.* **78,** 248–263 (2011).

8. Searles, J. A., Carpenter, J. F. & Randolph, T. W. The ice nucleation temperature determines the primary drying rate of lyophilization for samples frozen on a temperature-controlled shelf. *J. Pharm. Sci.* **90,** 860–871 (2001).

9. Kauppinen, A. *et al.* In-Line Multipoint Near-Infrared Spectroscopy for Moisture Content Quantification during Freeze-Drying. *Anal. Chem.* **85,** 2377–2384 (2013).

10. Barresi, A. A., Pisano, R., Rasetto, V., Fissore, D. & Marchisio, D. L. Model-Based Monitoring and Control of Industrial Freeze-Drying Processes: Effect of Batch Nonuniformity. *Dry. Technol.* **28,** 577–590 (2010).

11. Food and Drug Administration. International Conference on Harmonisation Q8. (2004). at <http://www.fda.gov/downloads/Drugs/Guidances/ucm073507.pdf>

12. Vervaet, C., Vercruysse, J., Remon, J. P. & De Beer, T. in *Encyclopedia of Pharmaceutical Science and Technology* (Taylor and Francis, 2013).

13. Jungbauer, A. Continuous downstream processing of biopharmaceuticals. *Trends Biotechnol.* **31,** 479–492 (2013).

14. Corver, J. A. W. M. Method and system for freeze-drying injectable compositions, in particular pharmaceutical. WO2013036107. (2013).

15. De Meyer, L. *et al.* Evaluation of spin freezing versus conventional freezing as part of a continuous pharmaceutical freeze-drying concept for unit doses. *Int. J. Pharm.* **496,** 75–85 (2015).

16. Bird, R., Stewart, W. & Lightfoot, E. in *Transport phenomena* (John Wiley & Sons, 2006).

17. Kuu, W. Y., Hardwick, L. M. & Akers, M. J. Rapid determination of dry layer mass transfer resistance for various pharmaceutical formulations during primary drying using product temperature profiles. *Int. J. Pharm.* **313,** 99–113 (2006).

18. Overcashier, D. E., Patapoff, T. W. & Hsu, C. C. Lyophilization of protein formulations in vials: Investigation of the relationship between resistance to vapor flow during primary drying and small-scale product collapse. *J. Pharm. Sci.* **88,** 688–695 (1999).

19. De Beer, T. R. M. *et al.* Importance of Using Complementary Process Analyzers for the Process Monitoring, Analysis, and Understanding of Freeze Drying. *Anal. Chem.* **81,** 7639–7649 (2009).

20. De Beer, T. R. M. *et al.* In-Line and Real-Time Process Monitoring of a Freeze Drying Process Using Raman and NIR Spectroscopy as Complementary Process Analytical Technology (PAT) Tools. *J. Pharm. Sci.* **98,** 3430–3446 (2009).

21. Eriksson, L., Johansson, E., Kettaneh-Wold, N., Wikström, C. & Wold, S. *Design of Experiments: Principles and applications*. (Umetrics, 2008).

22. Vercruysse, J. *et al.* Visualization and understanding of the granulation liquid mixing and distribution during continuous twin screw granulation using NIR chemical imaging. *Eur. J. Pharm. Biopharm.* (2013).

23. Eriksson, L. *et al. Multi- and megavariate data analysis part 1: Basic principles and*

applications. (Umetrics, 2006).

24. Pieters, S. *et al.* Raman spectroscopy and multivariate analysis for the rapid discrimination between native-like and non-native states in freeze-dried protein formulations. *Eur. J. Pharm. Biopharm.* **85,** 263–271 (2013).

25. Nellis, G. F. & Klein, S. A. in *Heat Transfer* (Cambridge University Press, 2009).

26. Pisano, R. *et al.* Quality by design: optimization of a freeze-drying cycle via design space in case of heterogeneous drying behavior and influence of the freezing protocol. *Pharm. Dev. Technol.* **18,** 280–295 (2013).

27. Fissore, D., Pisano, R. & Barresi, A. a. Advanced approach to build the design space for the primary drying of a pharmaceutical freeze-drying process. *J. Pharm. Sci.* **100,** 4922–33 (2011).

28. Workman, J. & Weyer, L. *Practical Guide to Interpretive Near-Infrared Spectroscopy*. (CRC Press, 2007).

29. Pieters, S. *et al.* Near-infrared spectroscopy for in-line monitoring of protein unfolding and its interactions with lyoprotectants during freeze-drying. *Anal. Chem.* **84,** 947–955 (2012).

30. Chen, R., Slater, N. K. H., Gatlin, L. A., Kramer, T. & Shalaev, E. Y. Comparative rates of freeze-drying for lactose and sucrose solutions as measured by photographic recording, product temperature, and heat flux transducer. *Pharm. Dev. Technol.* **13,** 367–374 (2008).

31. De Beer, T. *et al.* Near infrared and Raman spectroscopy for the in-process monitoring of pharmaceutical production processes. *Int. J. Pharm.* **417,** 32–47 (2011).

32. Mortier, S. T. F. C. *et al.* Uncertainty analysis as essential step in the establishment of the dynamic Design Space of primary drying during freeze-drying. *Eur. J. Pharm. Biopharm.* (2016). doi:http://dx.doi.org/10.1016/j.ejpb.2016.03.015

List of figures

'Mass of sublimed ice in 15 minutes' plotted in function of 'Distance between IR heaters and vial' *Dis* for high (blue) and low (green) level of 'Electrical power' *P*

Figure 5: Score scatter plot including the explanation of the chronological trends; each point represents one NIR spectrum

Figure 6: Loading line plot of PC 1 (black) and PC 2 (blue)

Figure 7: Visualization of drying progress with collected NIR spectra: (a) Progress primary drying: overwhelming ice bands until ice-free product became partially visible, (b) Progress primary drying: appearance of bands characteristic for trehalose and water (First inflection in point score plot), (c) Finalizing primary drying: decrease in ice band (Second inflection point in score plot), (d) Progress secondary drying: decrease in water band until completely dried product (Cluster of NIR spectra in score plot)

Figure 8: Scores of PC 1 in function of time: each point represents one NIR spectrum; time is expressed as number of spectra; one spectrum corresponds to 20 seconds of drying time

Figure 9: Extended coefficient plot DoE 2, response: total drying time: Regression coefficients displayed including 95% confidence interval, with electrical power (*P)*, distance between IR heaters and vial (*Dis*), thickness of the product layer (*Lpr*) and the expanded model terms related to the qualitative factor Formulation (*For(For1)*, *For(For2), For(For3), For(For4)* and *For(For5)*)

Figure 10: Extended coefficient plot DoE 2, response: primary drying time: Regression coefficients displayed including 95% confidence interval, with electrical power (*P)*, distance between IR heaters and vial (*Dis*), thickness of the product layer (*Lpr*) and the expanded model terms related to the qualitative factor Formulation (*For(For1)*, *For(For2), For(For3), For(For4)* and *For(For5)*)

Figure 11: Extended coefficient plot DoE 2, response: secondary drying time: Regression coefficients displayed including 95% confidence interval, with electrical power (*P)*, distance between IR heaters and vial (*Dis*), thickness of the product layer (*Lpr*) and the expanded model terms related to the qualitative factor Formulation (*For(For1)*, *For(For2), For(For3), For(For4)* and *For(For5)*)

Table 1:

Overview factors DoE 1 with lowest and highest level

	Level		
Factors	**-**	**+**	**Unit**
Quantitative			
Electrical power	14	36	W
Distance between IR heaters and vial	2	6	cm
Chamber pressure	10	30	Pa
Product layer thickness	0.5	1.5	mm
Qualitative			
Formulation	Formulation 1-5		

Table 2:

Overview experiments of DoE 1, the experiments in bold were performed twice (centre points)

Experiment number	Electrical power (W)	Distance heater-vial (cm)	Chamber pressure (Pa)	Layer thickness (mm)	Formulation
1	14	2	10	0.5	Formulation 1
2	36	6	10	0.5	Formulation 1
3	36	2	30	0.5	Formulation 1
4	14	6	30	0.5	Formulation 1
5	36	2	10	1.5	Formulation 1
6	14	6	10	1.5	Formulation 1
7	14	2	30	1.5	Formulation 1
8	36	6	30	1.5	Formulation 1
9	36	2	10	0.5	Formulation 2
10	14	6	10	0.5	Formulation 2
11	14	2	30	0.5	Formulation 2
12	36	6	30	0.5	Formulation 2
13	14	2	10	1.5	Formulation 2
14	36	6	10	1.5	Formulation 2
15	36	2	30	1.5	Formulation 2
16	14	6	30	1.5	Formulation 2
17	36	2	10	0.5	Formulation 3
18	14	6	10	0.5	Formulation 3
19	14	2	30	0.5	Formulation 3
20	36	6	30	0.5	Formulation 3
21	14	2	10	1.5	Formulation 3
22	36	6	10	1.5	Formulation 3
23	36	2	30	1.5	Formulation 3
24	14	6	30	1.5	Formulation 3
25	36	2	10	0.5	Formulation 4
26	14	6	10	0.5	Formulation 4
27	36	6	30	0.5	Formulation 4
28	36	6	10	1.5	Formulation 4
29	14	2	30	1.5	Formulation 4
30	36	2	30	1.5	Formulation 4
31	36	6	10	0.5	Formulation 5
32	36	2	30	0.5	Formulation 5
33	14	2	10	1.5	Formulation 5
34	14	6	10	1.5	Formulation 5
35	36	2	30	1.5	Formulation 5
36	36	6	30	1.5	Formulation 5
37	**25**	**4**	**20**	**1**	**Formulation 1**
38	**25**	**4**	**20**	**1**	**Formulation 5**

Table 3:

Overview of the five model formulations included as a qualitative factor in DoE 1 and 2

	Composition	
Formulation	**Component**	**Concentration**
Formulation 1	Trehalose	45 mg/mL
	Polysorbate 20	0.1 mg/mL
	Histidine	5 mM (pH 6)
Formulation 2	Lactose	30 mg/mL
	Sucrose	3.42 mg/mL
	Glycine	3.75 mg/mL
	NaCl	0.58 mg/mL
Formulation 3	Mannitol	30 mg/mL
	Sucrose	3.42 mg/mL
	Glycine	3.75 mg/mL
	NaCl	0.58 mg/mL
Formulation 4	Lactose	30 mg/mL
Formulation 5	Sucrose	30 mg/mL

Table 4:

Overview factors DoE 2 with lowest and highest level

	Level		
Factors	**-**	**+**	**Unit**
Quantitative			
Electrical power	14	36	W
Distance between IR heaters and vial	2	6	cm
Product layer thickness	0.5	1.5	mm
Qualitative			
Formulation	Formulation 1-5		

Table 5:

Overview experiments of DoE 2, the experiments in bold were performed twice (centre points)

Experiment number	Electrical power (W)	Distance heater-vial (cm)	Layer thickness (mm)	Formulation
1	14	2	0.5	Formulation 1
2	36	2	0.5	Formulation 1
3	36	6	0.5	Formulation 1
4	14	2	1.5	Formulation 1
5	36	2	1.5	Formulation 1
6	14	6	1.5	Formulation 1
7	36	6	1.5	Formulation 1
8	14	2	0.5	Formulation 2
9	36	2	0.5	Formulation 2
10	14	6	0.5	Formulation 2
11	36	6	0.5	Formulation 2
12	36	2	1.5	Formulation 2
13	14	6	1.5	Formulation 2
14	14	2	0.5	Formulation 3
15	36	2	0.5	Formulation 3
16	14	6	0.5	Formulation 3
17	14	2	1.5	Formulation 3
18	36	6	1.5	Formulation 3
19	14	2	0.5	Formulation 4
20	36	6	0.5	Formulation 4
21	14	2	1.5	Formulation 4
22	36	2	1.5	Formulation 4
23	14	6	1.5	Formulation 4
24	36	2	0.5	Formulation 5
25	14	6	0.5	Formulation 5
26	14	2	1.5	Formulation 5
27	36	2	1.5	Formulation 5
28	36	6	1.5	Formulation 5
29	**25**	**4**	**1**	**Formulation 1**
30	**25**	**4**	**1**	**Formulation 5**

Table 6:

Regression coding of the five-level qualitative factor formulation (*For*)

	Expanded term			
Level of factor	***For(For2)***	***For(For3)***	***For(For4)***	***For(For5)***
For1	-1	-1	-1	-1
For2	1	0	0	0
For3	0	1	0	0
For4	0	0	1	0
For5	0	0	0	1

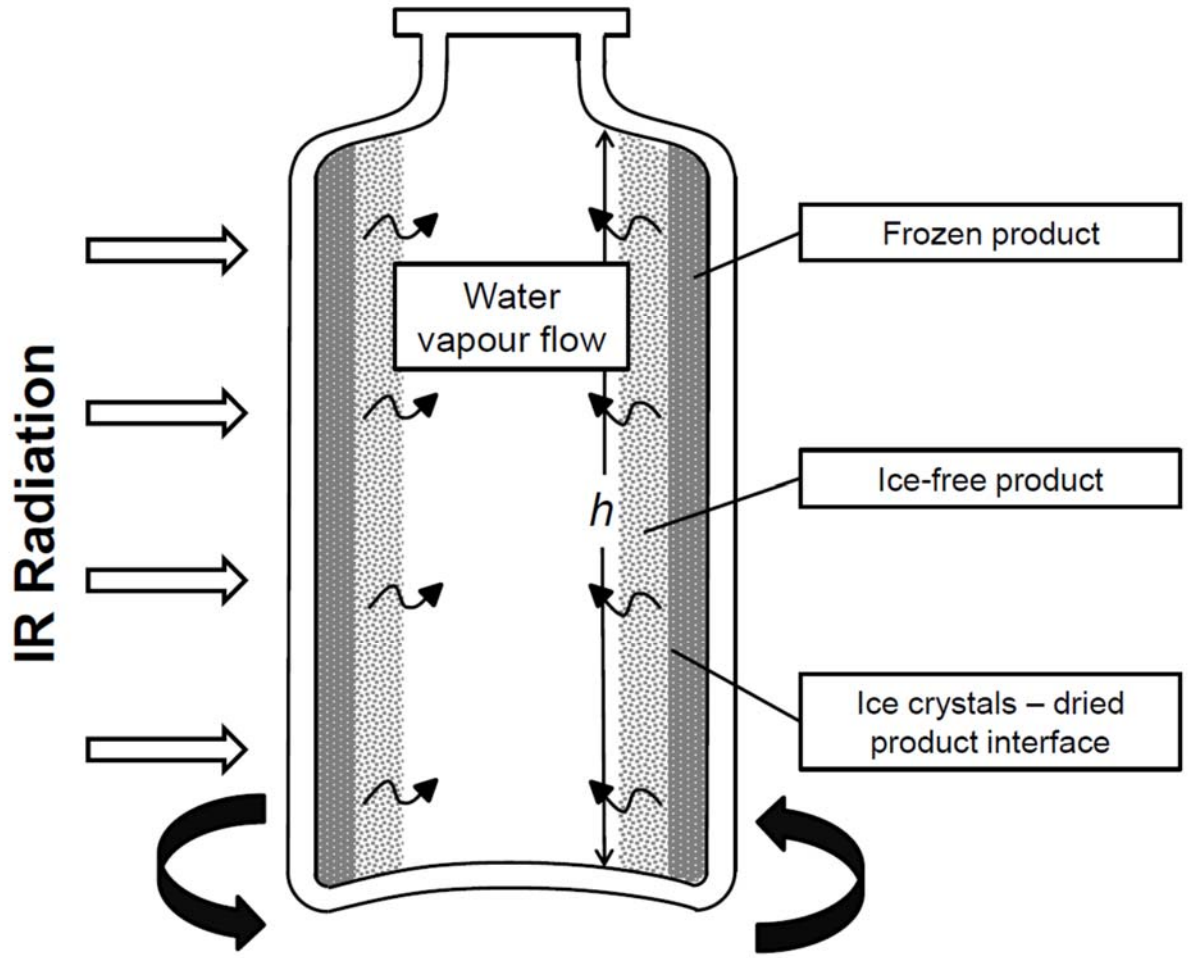

Figure 1: Illustration of IR mediated primary drying of spin frozen vials: IR radiation is provided to one side of the vial, which is slowly rotating along its longitudinal axis to assure homogeneous energy transfer

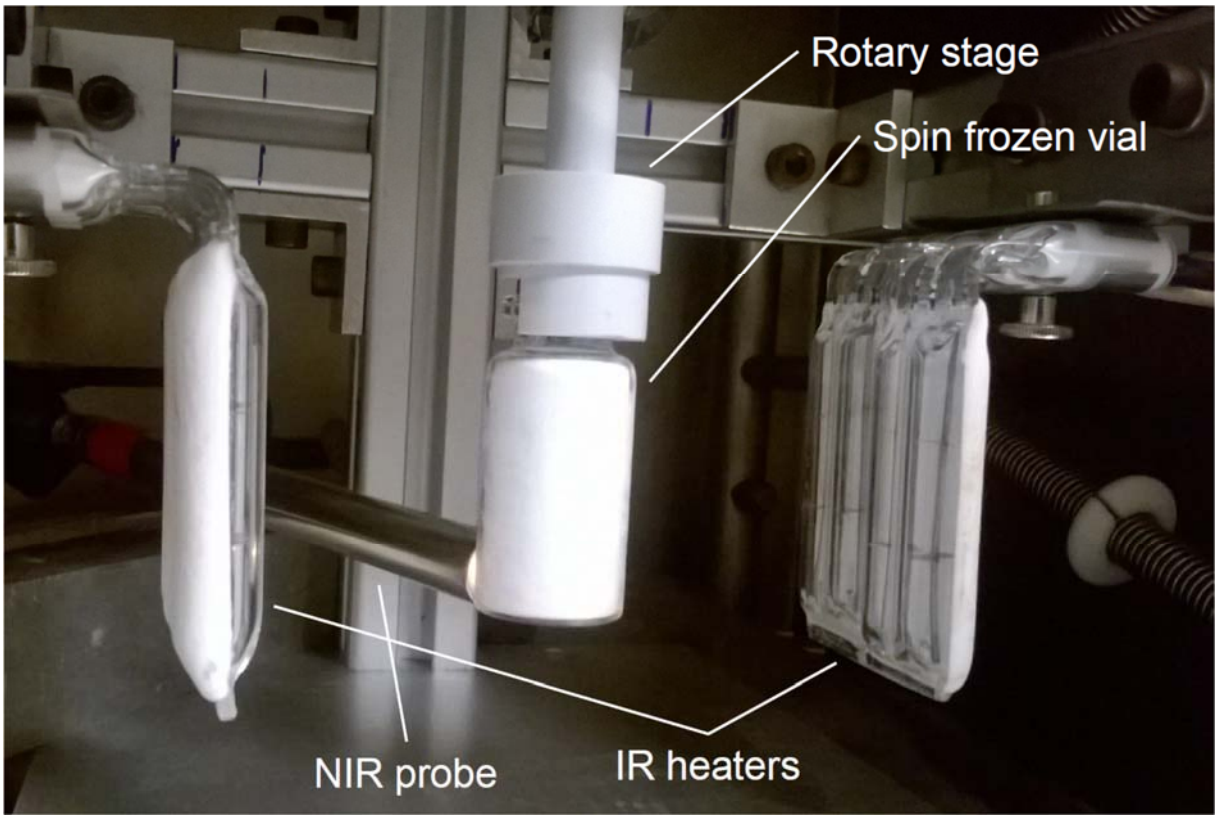

Figure 2: Experimental drying set-up with in-line NIR monitoring

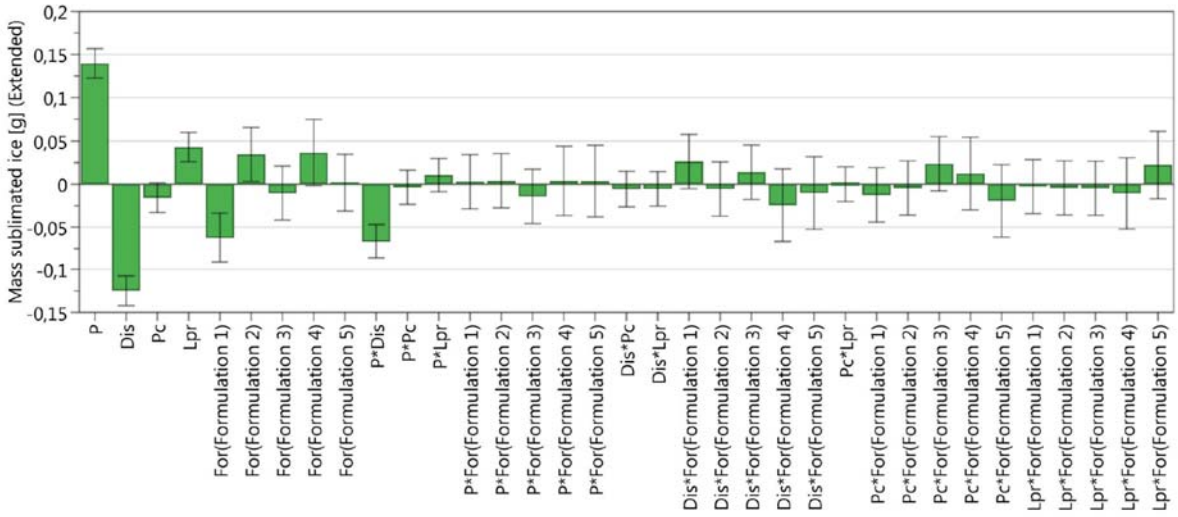

Figure 3: Extended coefficient plot DoE 1: Regression coefficients displayed including 95% confidence interval, with electrical power (*P)*, distance between IR heaters and vial (*Dis*), chamber pressure (*Pc*), thickness of the product layer (*Lpr*) and the expanded model terms related to the qualitative factor Formulation (*For(For1)*, *For(For2), For(For3), For(For4)* and *For(For5)*)

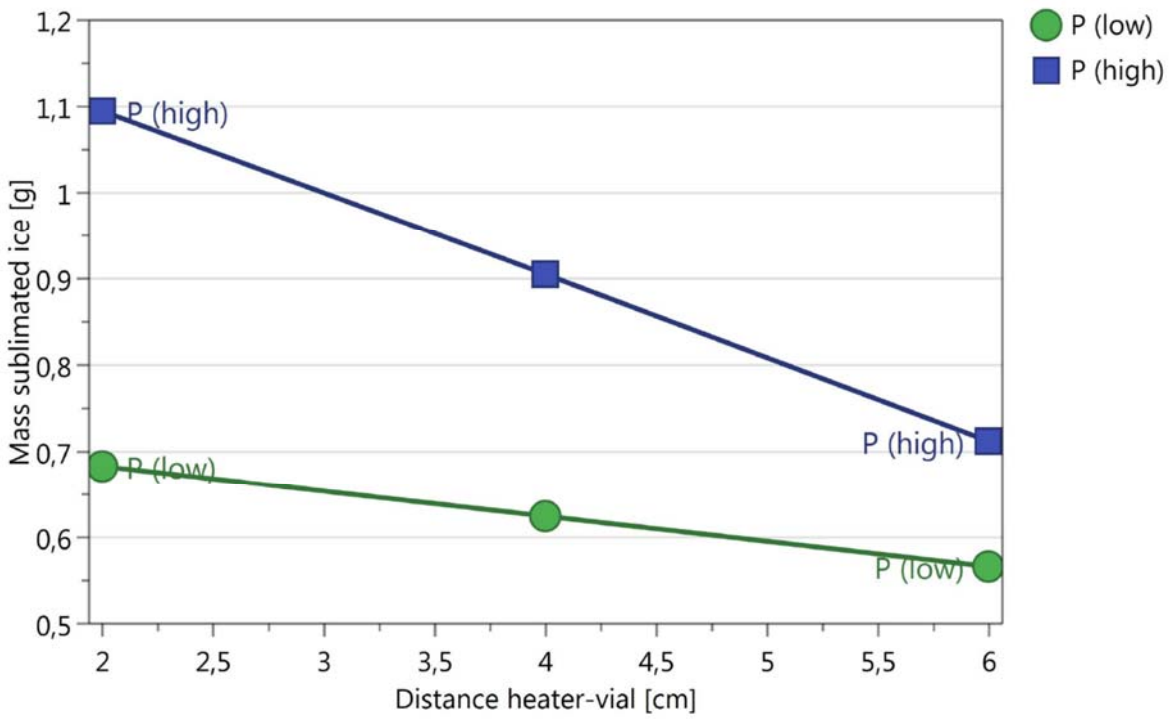

Figure 4: Interaction plot 'Electrical power'*'Distance between IR heaters and vial' (*P*Dis*): response 'Mass of sublimed ice in 15 minutes' plotted in function of 'Distance between IR heaters and vial' *Dis* for high (blue) and low (green) level of 'Electrical power' *P*

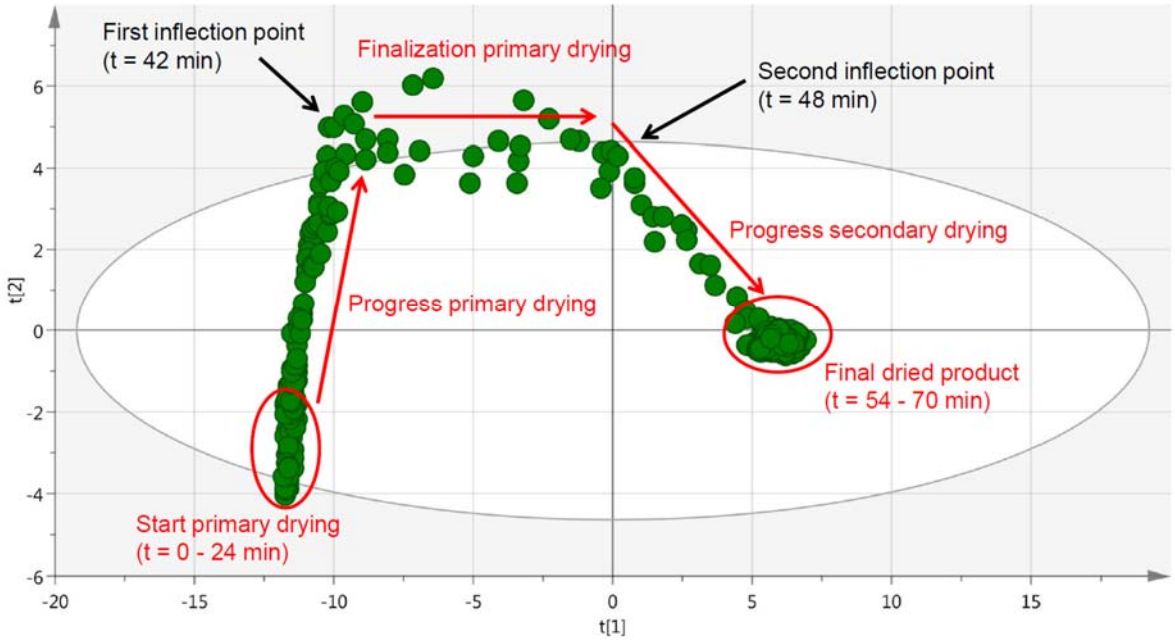

Figure 5: Score scatter plot including the explanation of the chronological trends; each point represents one NIR spectrum

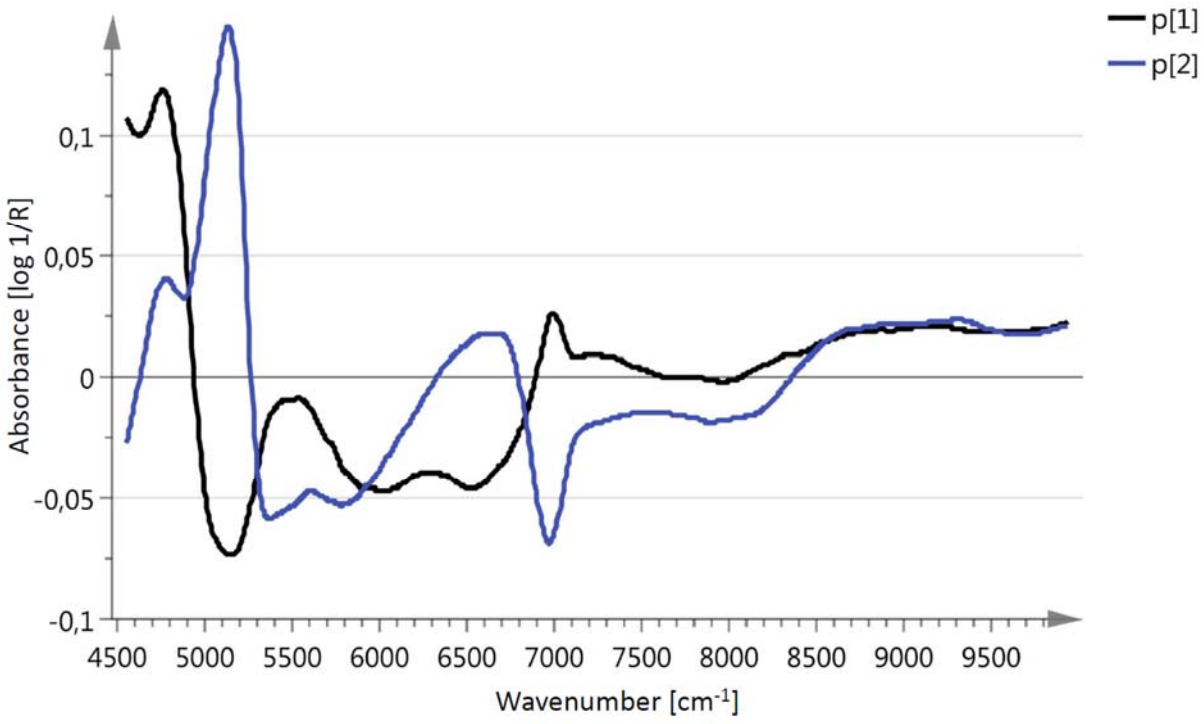

Figure 6: Loading line plot of PC 1 (black) and PC 2 (blue)

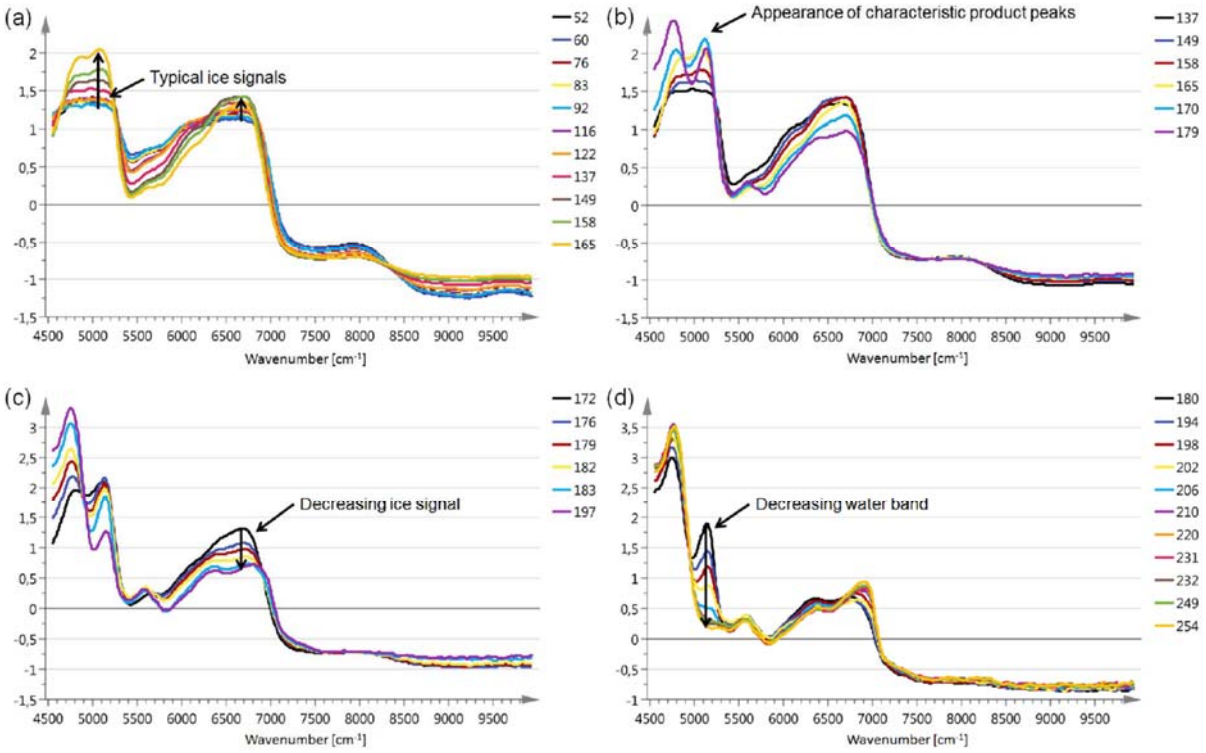

Figure 7: Visualization of drying progress with collected NIR spectra: (a) Progress primary drying: overwhelming ice bands until ice-free product became partially visible, (b) Progress primary drying: appearance of bands characteristic for trehalose and water (First inflection in point score plot), (c) Finalizing primary drying: decrease in ice band (Second inflection point in score plot), (d) Progress secondary drying: decrease in water band until completely dried product (Cluster of NIR spectra in score plot)

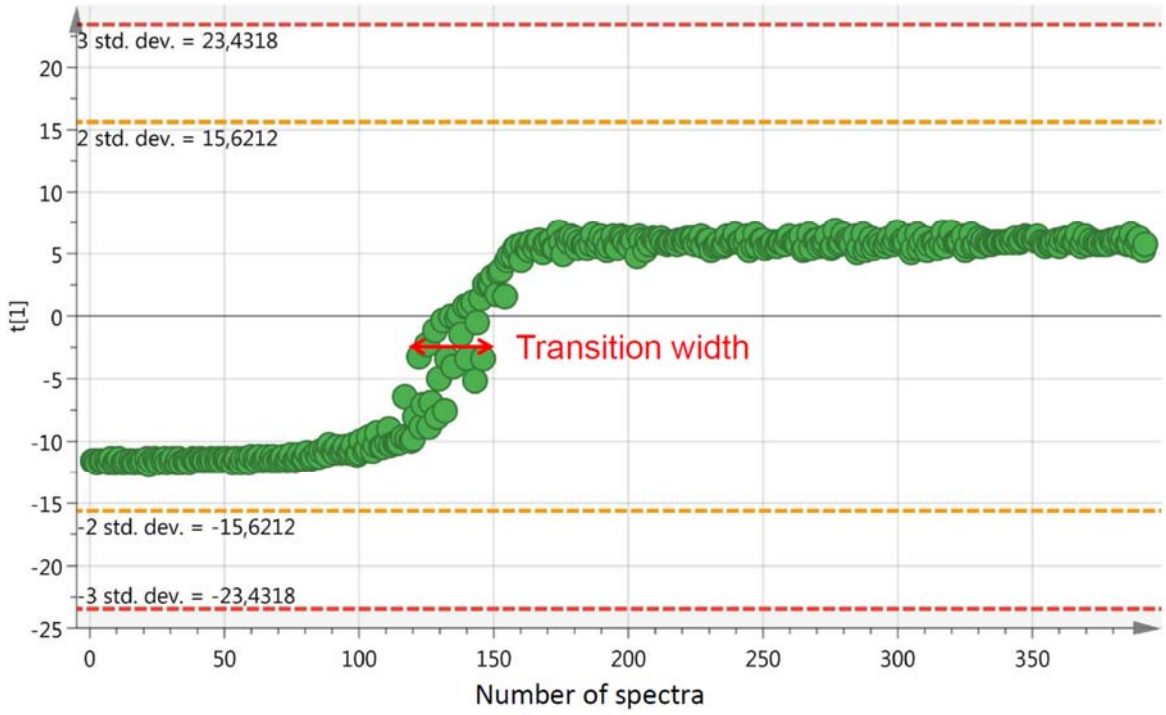

Figure 8: Scores of PC 1 in function of time: each point represents one NIR spectrum; time is expressed as number of spectra; one spectrum corresponds to 20 seconds of drying time

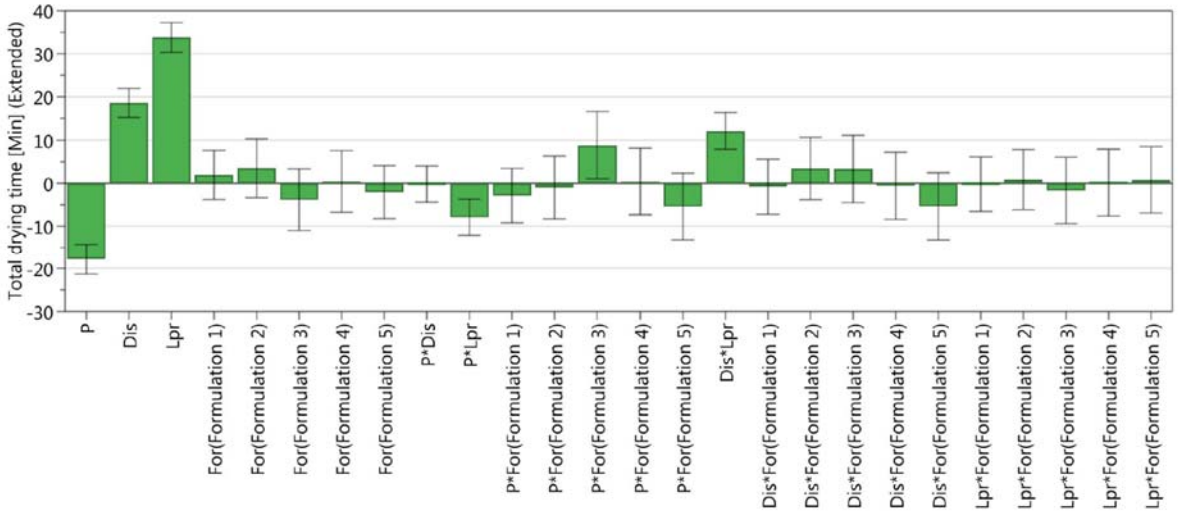

Figure 9: Extended coefficient plot DoE 2, response: total drying time: Regression coefficients displayed including 95% confidence interval, with electrical power (*P)*, distance between IR heaters and vial (*Dis*), thickness of the product layer (*Lpr*) and the expanded model terms related to the qualitative factor Formulation (*For(For1)*, *For(For2), For(For3), For(For4)* and *For(For5)*)

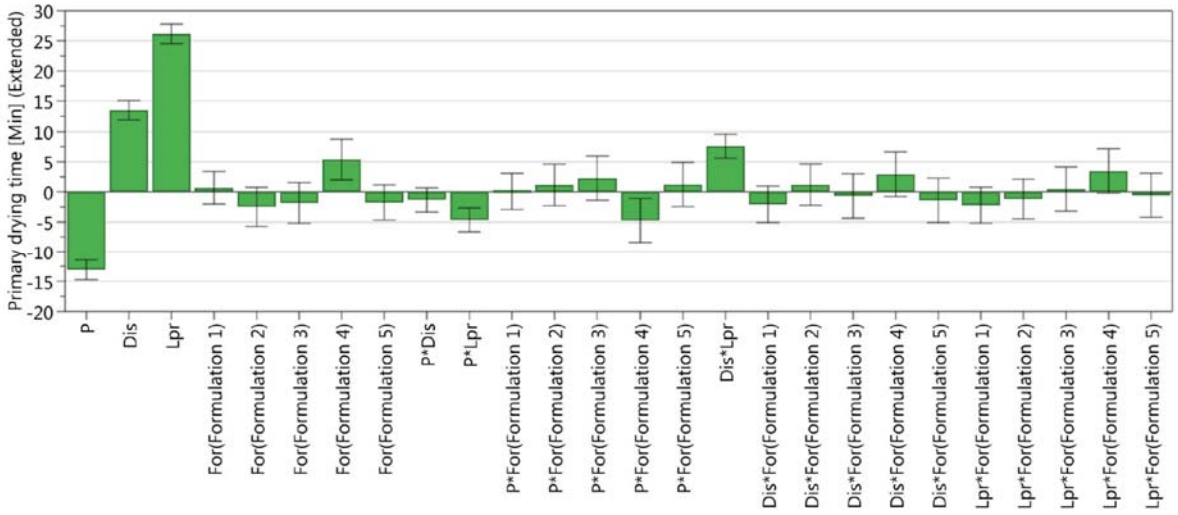

Figure 10: Extended coefficient plot DoE 2, response: primary drying time: Regression coefficients displayed including 95% confidence interval, with electrical power (*P)*, distance between IR heaters and vial (*Dis*), thickness of the product layer (*Lpr*) and the expanded model terms related to the qualitative factor Formulation (*For(For1)*, *For(For2), For(For3), For(For4)* and *For(For5)*)

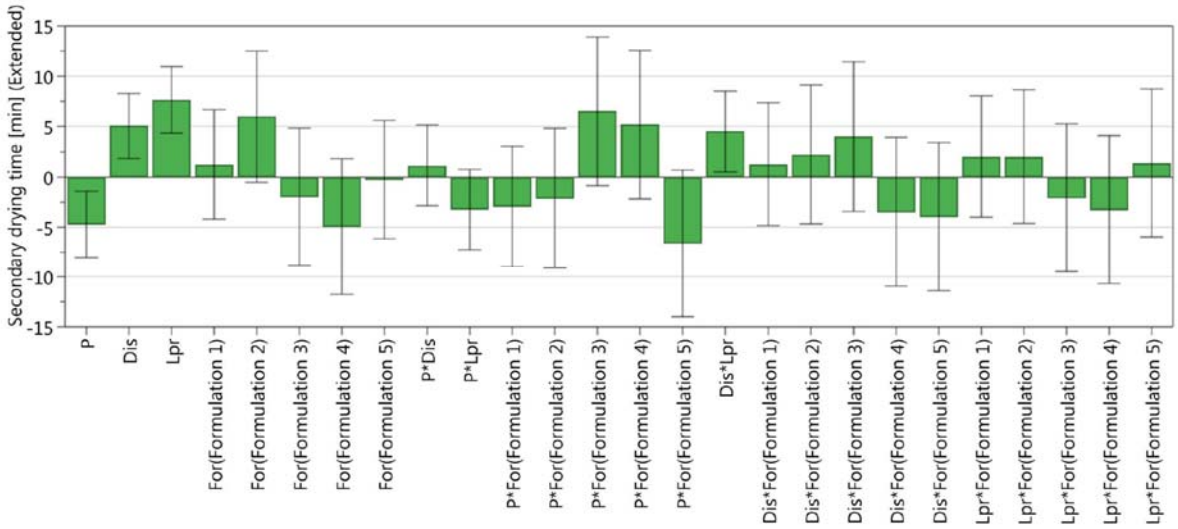

Figure 11: Extended coefficient plot DoE 2, response: secondary drying time: Regression coefficients displayed including 95% confidence interval, with electrical power (*P)*, distance between IR heaters and vial (*Dis*), thickness of the product layer (*Lpr*) and the expanded model terms related to the qualitative factor Formulation (*For(For1)*, *For(For2), For(For3), For(For4)* and *For(For5)*)